PAPER

Nanoscale potential fluctuations in nonstoichiometrics tantalum oxide

To cite this article: Vladimir A Gritsenko *et al* 2018 *Nanotechnology* **29** 425202

View the article online for updates and enhancements.

Related content

IOP ebooks™

Bringing you innovative digital publishing with leading voices to create your essential collection of books in STEM research.

Start exploring the collection - download the first chapter of every title for free.

Nanoscale potential fluctuations in nonstoichiometrics tantalum oxide

Vladimir A Gritsenko[1,2,3,5] ⓘ, Vladimir A Volodin[1,2] ⓘ,
Timofey V Perevalov[1,2] ⓘ, Vladimir N Kruchinin[1] ⓘ, Alina K Gerasimova[1] ⓘ,
Vladimir Sh Aliev[1] ⓘ and Igor P Prosvirin[4] ⓘ

[1] Rzhanov Institute of Semiconductor Physics SB RAS, 13 Lavrentiev ave., 630090, Novosibirsk, Russia
[2] Novosibirsk State University, 2 Pirogov str., 630090 Novosibirsk, Russia
[3] Novosibirsk State Technical University, 20 K. Marx ave., 630073, Novosibirsk, Russia
[4] Boreskov Institute of Catalysis SB RAS, 5 Lavrentiev ave., 630090, Novosibirsk, Russia

E-mail: grits@isp.nsc.ru

CrossMark

Abstract

The atomic and electronic structure of nonstoichiometric amorphous tantalum oxide (TaO_x) films of different composition has been investigated by means of electron microscopy, x-ray photoelectron spectroscopy, Raman and infrared spectroscopy. The dispersion of the absorption coefficient and refraction index has been studied by spectral ellipsometry. The optical spectra were interpreted using the results of a quantum-chemical simulation for crystalline orthorhombic TaO_x. It was found that the presence of oxygen vacancies in the oxygen-deficient TaO_x film show an optical absorption peak at 4.6 eV. It has been established that TaO_x consists of stoichiometric Ta_2O_5, metallic Ta clusters less than 20 nm in size, and tantalum suboxides TaO_y ($y < 2.5$). The model of nanoscale potential fluctuations of TaO_x bandgap in the range of 0–4.2 eV is proposed and justified. The design of the flash memory element based on the effect of localization of electrons and holes in Ta metallic nanoclusters in the TaO_x matrix is proposed.

Keywords: tantalum oxide, nanoscale potential fluctuations, ellipsometry, x-ray photoelectron spectroscopy, Raman scattering, density functional theory, ReRAM

(Some figures may appear in colour only in the online journal)

Introduction

Stoichiometric tantalum oxide (Ta_2O_5) films have a high value of dielectric constant (κ in the range of 20–50), and they are used as dielectrics in the storage capacitors of dynamic memory devices [1–4]. Recently Ta_2O_5 are examined as a storage medium in charge trap flash (CTF) memory devices [5]. Oxygen vacancies in oxides and nitrogen vacancies in nitrides (for example in Si_3N_4 films) are used as traps in those devices. It is believed that oxygen vacancies play a key role in dielectric reversible switching between states with low and high resistance under current pulse (resistive effect). Intensive studies aimed at the development of resistive random-access memory (ReRAM) are carried out now. ReRAM have attracted great attention due to their

simple structure, low power consumption, high-speed operation, high-density integration, multibyte switching. A number of binary metal oxides have been investigated for ReRAM applications. Nonstoichiometric tantalum oxide (TaO_x) is one of the promising materials for ReRAM [6–8]. It was suggested that oxygen vacancies are responsible for the charge localization in Ta_2O_5 and TaO_x [9, 10]. Recently we have shown that charge transport in ReRAM based on metal suboxides was interpreted in terms on electron percolation in the suboxides [11–13]. Percolation in metal suboxides is related to nanoscale potential fluctuations due to chemical composition (stoichiometry) fluctuations.

Variation of the chemical composition, or stoichiometry, of TaO_x results in a modification of its electronic structure; this knowledge opens up a possibility for exerting control over the physical (optical and electrical) properties of the material. The dependence of the Ta coordination number as a function of

---

[5] Author to whom any correspondence should be addressed.

Table 1. TaO_x films synthesis conditions, composition (atomic ratio [O]/[Ta]) according to XPS data, and optical properties according to ellipsometry data.

Sample	$P(O_2)$, 10^{-3} Pa	x = [O]/ [Ta]	Optical properties of TaO_x, E = 1.96 eV	
			n	α, (cm^{-1}), $\times 10^{-6}$
T1	0.53	1.94	3.614	0.510
T2	1.08	1.99	3.057	0.406
T3	1.35	2.13	2.792	0.307
T4	1.71	2.22	2.692	0.242
T5	2.21	2.44	2.530	0.137
T6	2.81	2.59	2.476	—
T7	3.49	2.79	2.246	—
T8	9.09	2.77	2.089	—
Мет.	—	—	1.734	0.414

stoichiometry parameter x was investigated in [14]. In Ta_2O_5, the Ta coordination number is 6, which corresponds the structural unit TaO(6) octahedrons. Oxygen atoms are coordinated with two or three tantalum atoms. The structure of nonstoichiometric metal-enriched TaO_x can be described in framework of the random mixture (RM) or random bonding (RB) models [15]. In the RM model, TaO_x is treated as a mixture of two phases: the stoichiometric phase Ta_2O_5 and the metallic Ta. In the RB model, TaO_x is assumed to consist of $TaO(\nu)$–$Ta(6-\nu)$ structural units, ν = 0, 1, 2, 3, 4, 5, and 6, in which Ta atoms statistically substitute O atoms in each TaO(6) structural unit.

The purpose of the present work was the justification of nanoscale potential fluctuation model in nonstoichiometric tantalum oxides. To reach this purpose the studies of the atomic and electronic structure of TaO_x by means of x-ray photoelectron spectroscopy (XPS), spectral ellipsometry, Raman spectroscopy, IR-spectroscopy, were carried out. Quantum-chemical simulations were performed to calculate energy level of oxygen vacancies in crystalline tantalum oxide for interpretation of experimental data.

Methods

The ion-beam sputtering-deposition (IBSD) technique was used to deposit onto the surface of phosphorous-doped Si (100) wafers with resistivity 4.5 Ohm·cm a series of TaO_x films of different stoichiometries x with thicknesses in the range from 10 to 50 nm. Prior to the film growth, the silicon substrates were cleaned in a solution of hydrofluoric acid (HF). For sputtering, a metallic tantalum target was used. The target was sputtered with 1.2 keV Ar$^+$ ions. Simultaneously, high-purity oxygen was let into the chamber (O_2 > 99.999 atomic %). The partial oxygen pressure ($P(O_2)$) in the growth zone was varied within the interval 0.5 ÷ 9.1 × 10^{-3} Pa; as a result, tantalum oxide films with different compositions x (or Ta/O ratios) were grown: from near-stoichiometric composition ($x \approx 5/2$) to nonstoichiometric TaO_x ($x < 5/2$) (see table 1). Eight samples (T1–T8) of various stoichiometry

were grown (see table 1). The $P(O_2)$ decreased from sample T8 to sample T1.

For studying the surface morphology of TaO_x films, the method of field emission scanning electron microscopy (FESEM) implemented on a Zeiss 1540 Crossbeam system instrument was employed. The XPS spectra of TaO_x films were measured on a SPECS (Germany) photoelectron spectrometer using a hemispherical PHOIBOS-150-MCD-9 analyzer and FOCUS-500 monochromator (Al Kα radiation, $h\nu$ = 1486.74 eV, 200 W). The spectra were registered at the analyzer pass energy of 20 eV. The sampling depth is about 6.6 nm. The line shape used for fitting the Ta 4f spectra was the product of Lorentzian and Gaussian functions. A Shirley-type background was subtracted from each spectrum. The [O]/[Ta] atomic ratio for samples were calculated from the integral photoelectron peak intensities, which were corrected with the theoretical sensitivity factors based on Scofield photoionization cross sections.

For ellipsometric analysis, ELLIPS-1891-SAG spectral ellipsometer (ISP SB RAS) was used [16]. The measurements of the spectral dependences of the ellipsometric angles Ψ and Δ were performed in the range of wavenumbers 250–1100 nm. The spectral resolution of the instrument was 2 nm, the record time of one spectrum did not exceed 20 s, and the angle of light incidence onto the sample was 70°. A four-probe measurement procedure with subsequent averaging of measured data over all the four zones was used. For determination of the thickness of transparent TaO_x films, multi-angle measurements performed on an LEF-3M ellipsometer at some chosen angles of light incidence onto the sample (50, 60, and 70°) were employed; the light wavelength in those measurements was λ = 632.8 nm. The recorded spectra of $\Psi(\lambda)_{exp}$ and $\Delta(\lambda)_{exp}$ were then used for solving the ellipsometry inverse problem and for fitting the experimental spectral dependences of ellipsometric angles $\Psi(\lambda)_{calc}$ and $\Delta(\lambda)_{calc}$ with the dependences calculated in accordance with the fundamental equation of ellipsometry.

For the ellipsometric calculations, the following optical models were used in the present study: the model of a semi-infinite reflecting system and that of a single-layer reflecting system. The adjustment of the spectral dependences of polarization angles throughout the whole spectral range for m spectrum points was implemented by minimization of the function:

$$\sigma^2 = \frac{1}{m} \cdot \sum_{i=1}^{m}[(\Delta_{exp.} - \Delta_{calc.})^2 + (\Psi_{exp.} - \Psi_{calc.})^2]. \quad (1)$$

In the calculations, the optical characteristics of silicon were borrowed from the database compiled by Adachi [17]. The dispersion dependence $n(\lambda)$ for TaO_x films was represented with a polynomial Cauchy dependence [18, 19]:

$$n(\lambda) = a + \frac{b}{\lambda^2} + \frac{c}{\lambda^4}, \quad (2)$$

where a, b, and c are adjustment coefficients.

Structural properties of TaO_x films were investigated by means of vibration spectroscopy (Raman and infrared (IR) absorbance). Raman spectra were registered at room temperature in back-scattering geometry. For excitation, the 514.5 nm line of an Ar$^+$ laser was used. No polarization

analysis for scattered light was performed. A Horiba Jobin Yvon T64000 spectrometer was used for measuring Raman spectra with a spectral resolution better than $2 \, \text{cm}^{-1}$. A special facility for microscopic Raman studies was also employed. The laser-beam power falling onto the sample was 2 mW. For minimization of the heating of the structures under the laser-beam, the sample was placed somewhat below the focus in a situation in which the laser-spot size was equal to 8 μm. The samples were studied using Fourier transform infrared (FTIR) absorption spectroscopy, the spectrometer FT-801 having a spectral resolution of $4 \, \text{cm}^{-1}$ was used.

Quantum-mechanical simulation of the tantalum oxide electronic structure was carried out in Quantum-ESPRESSO program package in framework of the density functional theory in the periodical supercell model [20]. The calculations were made for the orthorhombic λ-Ta_2O_5 because for this crystal phase the electronic structure of the material bulk as well as that of O vacancies was the same as the electronic structure for amorphous tantalum oxide [21, 22]. In the structure of λ-Ta_2O_5, Ta atoms are six-fold coordinated ones and O atoms occur as atoms of three types: two- and three-fold coordinated ones in the plane of Ta atoms, and two-fold coordinated ones in the plane of O atoms. The minimum formation energy of oxygen vacancies is that for the two-fold coordinated O in the Ta plane. The hybrid Becke–Lee–Yang–Parr exchange-correlation functional was used. The wavefunctions of valence electrons were decomposed in plane-wave basis set with 950 eV cutoff energy, with the core being considered through normconserving pseudopotentials. In the calculations, the following electronic configurations were used: Ta: $[Xe]5d^36s^26p^0$ and O: $[He]2s^22p^4$. The cutoff energy was chosen such that to obtain a convergence not worse than $0.006 \, \text{eV/atom}$ in terms of total energy. Oxygen vacancies were produced by the removal of O atom from 168-atom supercells obtained by $2 \times 2 \times 3$ translation of a 14-atom unit cell along the crystallographic axes with subsequent relaxation of all atoms with force convergence threshold $0.04 \, \text{eV} \cdot \text{Å}^{-1}$.

Results

XPS spectra of the Ta 4f levels in TaO_x films of different composition as well as the results of curve-fitting analysis are shown in figure 1. XPS Ta 4f peak consists of the single spin–orbit doublet Ta $4f_{5/2,7/2}$ with the 1.89 eV splitting for the tantalum oxide grown at the highest $P(O_2)$ in the growth zone and it is observed at an energy corresponding to the Ta_2O_5 [23]. New peaks in the Ta 4f spectra at the lower binding energy are observed for films synthesized with lower $P(O_2)$, which corresponds to a partially reduced oxide and metallic Ta. The XPS for our TaO_x film are described by three doublets that can be attributed to Ta^{1+}, Ta^{2+}, Ta^{3+}/Ta^{4+}, and Ta^{5+}, respectively [23]. The Ta $4f_{7/2}$ binding energy of 21.25 eV related to metal Ta, 22.41 eV and 24.54 eV related to TaO_y, and 25.95 eV related to Ta_2O_5. Thus, the high-, intermediate- and low-energy XPS Ta 4f doublets are due to stoichiometric Ta_2O_5, nonstoichiometric suboxides (hereinafter referred to as $TaO_{y<2.5}$) and metallic Ta, respectively.

The atomic ratio $x = [O]/[Ta]$ are presented in table 1. We assume that nonstoichiometric films differ from each other in the relative content of Ta_2O_5, TaO_y and Ta. The quantitative accuracy in determining the oxide stoichiometry from the XPS data typically amounts about 10%. For this reason, the overestimated values of $x > 2.5$ are observed for T6, T7, T8 samples, which should be close to stoichiometric Ta_2O_5 while the T6 is slightly depleted in oxygen. The inflated value of the oxygen content in our tantalum oxide films is most likely due to the presence of adsorbed oxygen on the films surface.

The similar result was previously obtained for non-stoichiometric IBSD hafnium oxide films [24]. However, in that case the FESEM images revealed the presence of 10–80 nm metal clusters spread throughout the film. FESEM images of the TaO_x films look quite homogeneous on the scale shown in the figure 2. It seems that metallic Ta clusters in TaO_x were indistinguishable because the sizes of those clusters were much smaller than the sizes we could see with the help of FESEM. Figure 1 suggests that the sizes of metallic Ta clusters in the TaO_x films did not exceed 20 nm.

The spectral dependence of the optical absorption coefficient α of TaO_x films is shown in figure 3. The sample T8 is a dielectric whose fundamental absorption edge corresponded to the 4.2 eV, being coincident with the Ta_2O_5 bandgap [25]. Enrichment of TaO_x with the metal is accompanied with a red shift of the fundamental absorption edge. In sample T7, the absorption edge was located at 2.5 eV, and in sample T6 it was shifted to 2.0 eV. The spectral dependence of the absorption coefficient of TaO_x exhibited an intricate behavior. At a high enrichment of TaO_x with metal, features resembling those for metallic tantalum were observed. In sample T6, an absorption peak at 4.6 eV was observed. In sample T5, a kink of the derivative was observed at about 4.6 eV energy. On increasing the metal enrichment degree, the absorption coefficient α grew in magnitude, and at partial oxygen pressures of 1.35×10^{-3} Pa (sample T3) and 1.08×10^{-3} Pa (sample T2) the absorption spectrum started displaying an absorption peak at about 3.1 eV. Possible emergence of absorption peaks will be discussed below.

The dispersion of the refraction index n in TaO_x films of different composition is shown in figure 4. In the films with a low content of excessive Ta (T6–T8), a normal dispersion is observed: the n increases with increasing the photon energy. In TaO_x films with a high content of the excessive Ta (T1–T3), an anomalous dispersion is observed. At low photon energies, a decrease of n with increasing photon energy is observed. At high photon energies, the n increases in value with increasing the photon energy. In the films T1–T3, at photon energies in the range from 3 to 5 eV the spectral dependence of the n was close to that for the metal. In the low-energy region, at photon energies smaller than 3 eV, the n in the metal decreases from 2.8 to 1.0. In TaO_x samples T1–T5, unlike in the metal, the n decreases in value as the photon energy increases from 1.3 to 3.0 eV. Elucidation of the reasons for the observed contradiction calls for further studies.

For revealing the absorption peaks nature, we have carried out a quantum-chemical simulation of the electronic structure of the isolated O vacancy. The calculated spectra of
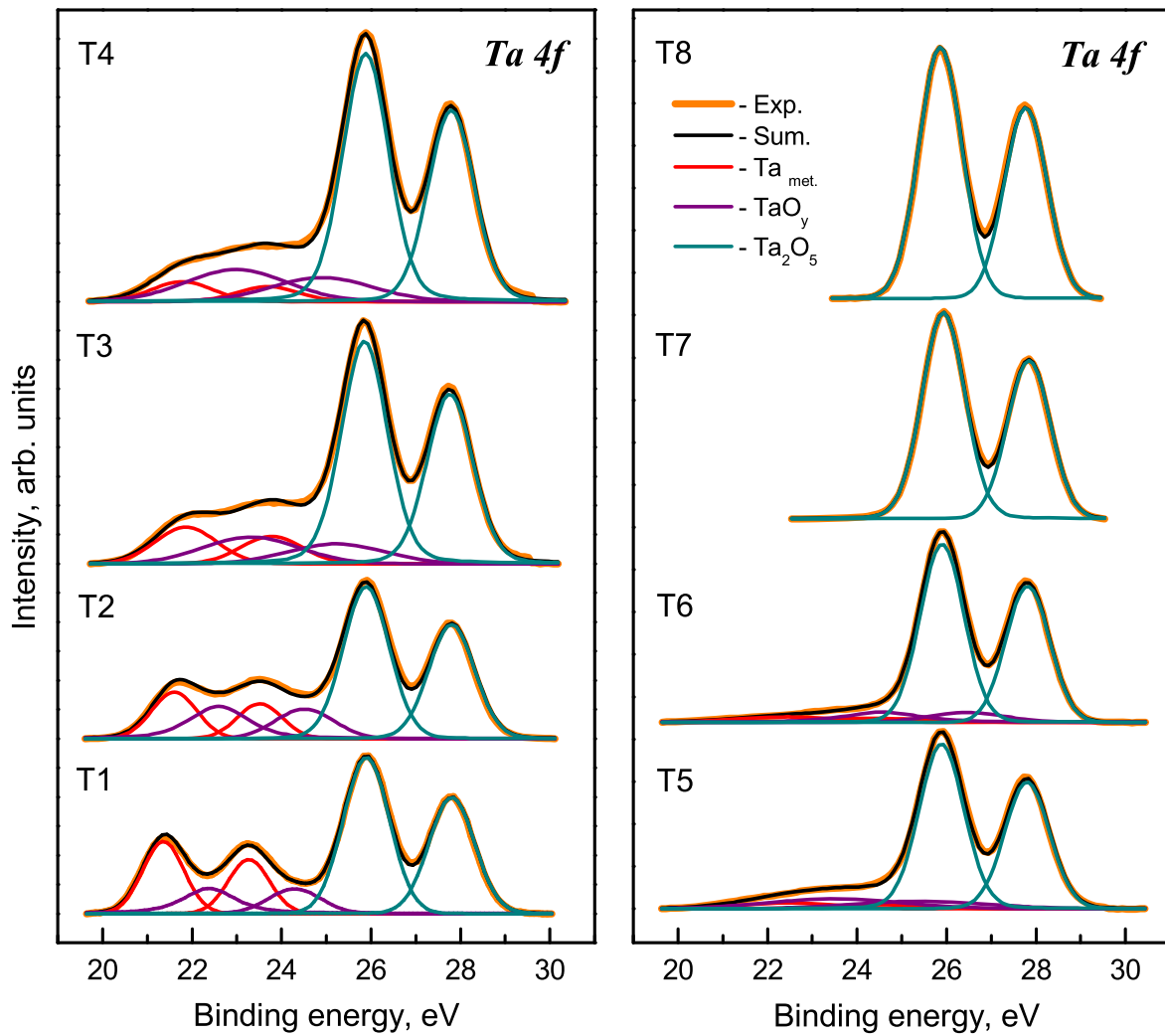
Figure 1. XPS Ta 4*f* levels of TaO$_x$ films of different compositions (orange lines) and their fitting with a superposition of Gaussian functions in the energies of the Ta 4*f* level (the red, violet, and blue lines refer to the various phases, the black line being the sum of the 'colored' components).
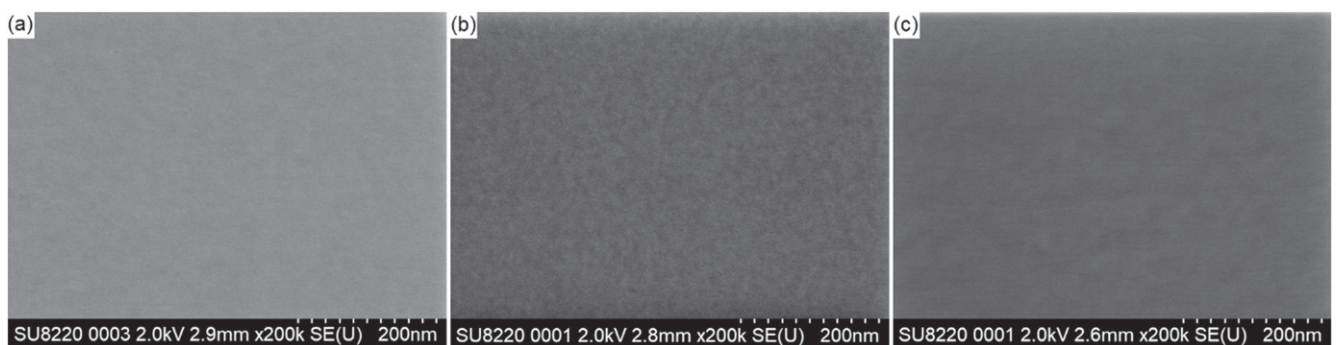

Figure 2. FESEM images of TaO$_x$ films grown at different partial oxygen pressures $P(O_2)$: 1.08×10^{-3} Pa (a), 1.35×10^{-3} Pa (b) and 2.21×10^{-3} Pa (c).

the projected density of electronic states from the Ta atoms closest to the O vacancy show that the vacancy forms an occupied defect state in the bandgap at 2.4 eV higher than the valence-band top (E_v) energy (figure 5) [26]. The defect state is formed predominantly by Ta 5*d* electrons with substantial contributions of Ta 6*s* and Ta 6*p*. The calculated spectrum predicts the possibility of optical transitions at the O vacancy with energies 4.5 and 4.65 eV from the defect level in the bandgap to the Ta 6*p*/Ta 6*s* and Ta 5*d* state in the conduction-band, respectively. The energy of those transitions agrees with the experimental 4.6 eV peak of the optical absorption spectra of TaO$_x$ slightly enriched with the metal for the T6
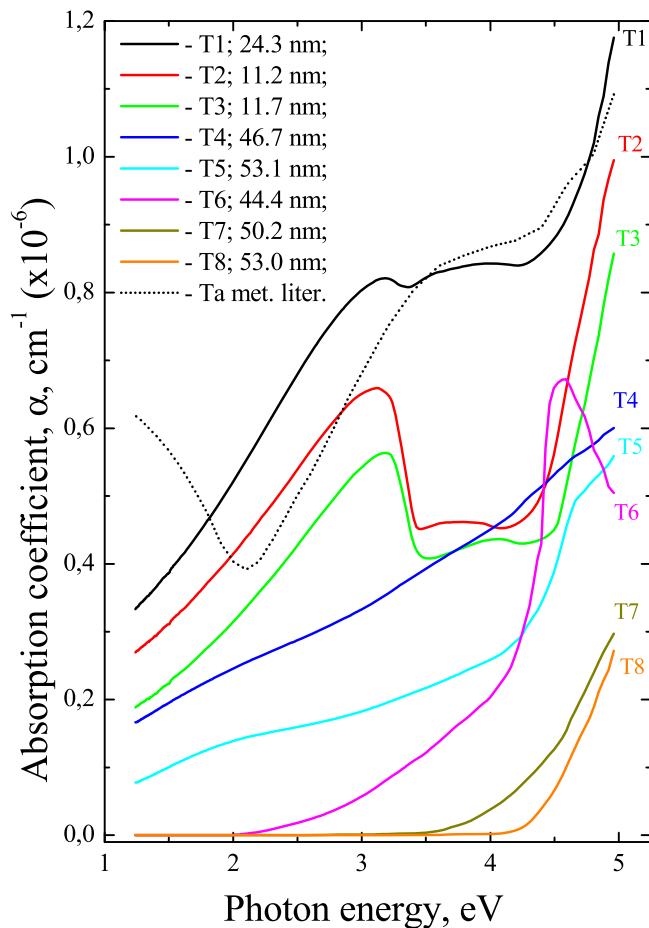
Figure 3. Spectral dependence of absorption coefficient in TaO$_x$ films of various compositions.

Figure 4. Spectral dependence of refraction index n in TaO$_x$ films of different compositions.

sample. Thus, this peak originated from the optical transitions in O vacancies. Interestingly, the calculations also predict transitions with energies 3.65 and 5.27 eV. In the optical absorption spectra of TaO$_x$, no features at those quantum energies were observed, most likely, due to the small values of the matrix elements for these transitions. The above-mentioned 3.1 eV peak (figure 3) in the absorption spectra of samples T2 and T3 can be attributed to the possible excitation of O vacancies (see figure 5) or with the excitation of O polyvacancies.

Measured Raman spectra of the TaO$_x$ films and the Raman spectrum of a silicon substrate are shown in figure 6. Evidently, a very intense signal due to silicon substrate is observed; this is a line due to the 520.6 cm^{-1} long-wave optical phonon. For clarity, the vertical scale is plotted logarithmic. Besides, features originating from two-phonon scattering phenomena, namely those due to events involving two acoustic phonons (2TA $\sim$300 cm^{-1}, LA + TA $\sim$425 cm^{-1}), optical plus acoustic phonon (O + A $\sim$600–700 cm^{-1}) and two optical phonons (2LO $\sim$800 cm^{-1} and 2TO $\sim$970 cm^{-1}) were observed in the spectrum of single-crystal silicon. TaO$_x$ films are semi-transparent ones in the visible light, and their spectrum also exhibits a signal due to the substrate. In the absorbing films (samples T1–T6, table 1), a weak signal due to the substrate is observed. In the transparent films (T7 and T8), the signal due to the substrate was somewhat
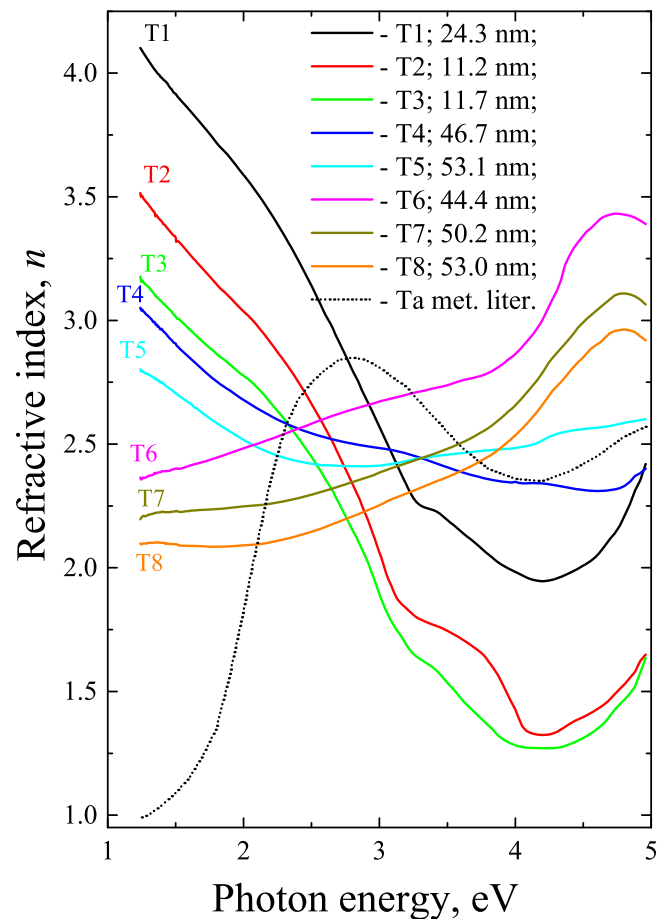

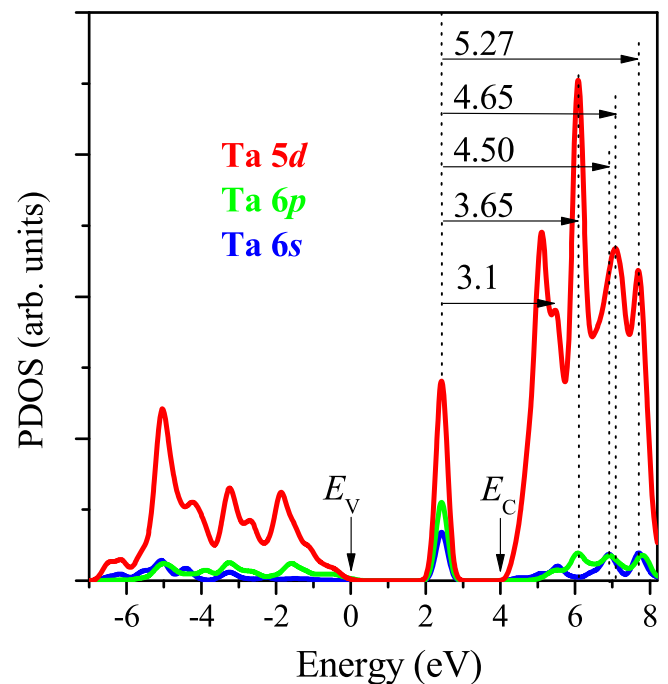**Figure 5.** The overall PDOS from the tantalum atoms closest to the neutral O vacancy in the 168-atom supercell of λ-Ta$_2$O$_5$: Ta 5d (red curve), Ta 6p (green curve) and Ta 6 s (blue curve). The energy is reckoned from the valence-band top.
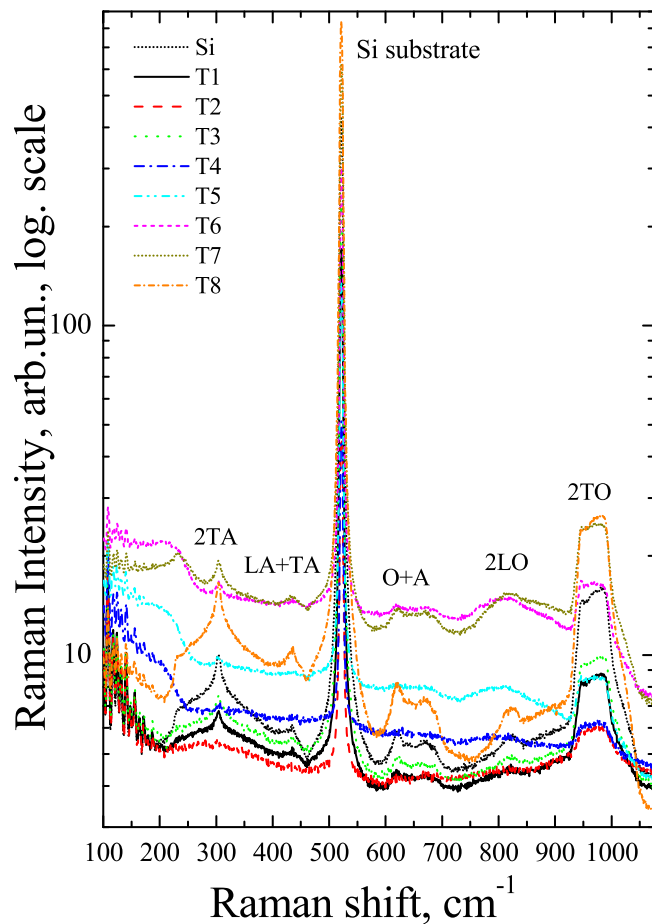
Figure 6. Raman spectra of TaO$_x$ films (T1–T8) and Si substrate.

Figure 7. Raman spectra of TaO$_x$ films (T1–T8) after subtraction of the contribution due to the Si substrate.

stronger because the film in that case acted as an anti-reflection coating. The narrow peaks with wavenumbers greater than 150 cm^{-1} resulted from the inelastic scattering of light by atmospheric molecules. It is seen that the features at about 200 and 800 cm^{-1} were also present in the spectra of TaO$_x$ films. In the spectra of amorphous Ta$_2$O$_5$, features due to the density of-state maximum observed in the density of vibrational states in the range of wavenumbers 600 to 1000 cm^{-1} were present [27–30]. The latter features correspond to the frequencies of Ta–O bond vibrations. Likely, the peak at $\sim$800 cm^{-1} is due to the light scattering by the vibrations of those bonds. The Raman signal of the film can be examined after subtraction of the signal due to substrate.

The Raman spectra of TaO$_x$ films after subtraction of the contribution due to silicon substrate are shown in figure 7. In the spectra, features at wavenumbers $\sim$200 cm^{-1}, $\sim$480 cm^{-1}, $\sim$600 cm^{-1}, and $\sim$800 cm^{-1} are observed.

Takashi Tsuchiya *et al* [27] also observed the majority of those Raman features as well as their evolution with decreasing the oxygen content of TaO$_x$ films of different stoichiometric compositions. The peaks at about 800 cm^{-1} were induced by the Ta–O valence (stretching) vibrations in the case in which the tantalum atoms were five-fold coordinated ones (i.e. each tantalum atom was surrounded by five O atoms). According to the assumptions of [27], in the case in which the tantalum atoms are six-coordinated, the Ta–O valence vibrations are manifested as
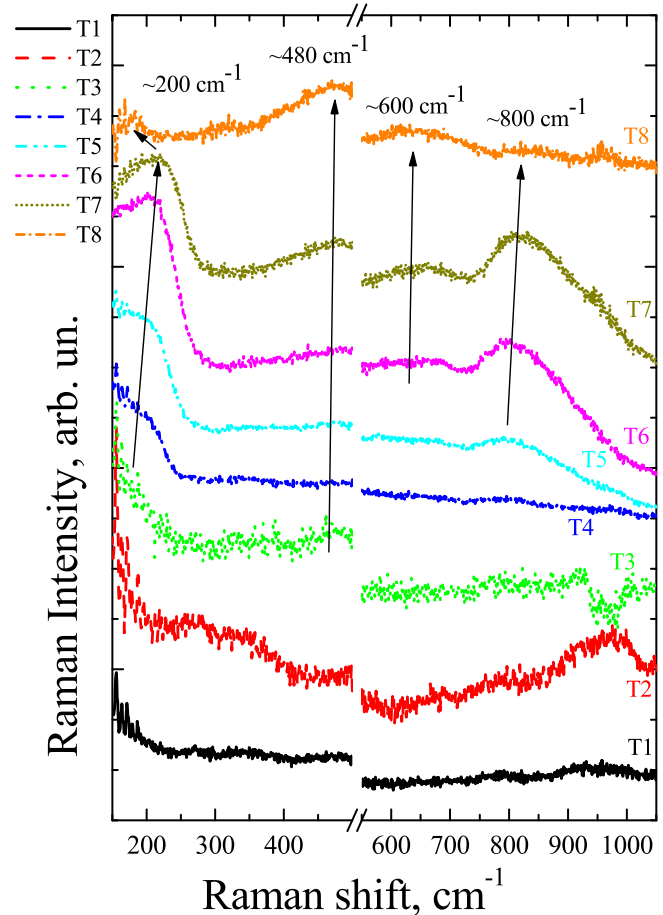
peaks with wavenumbers ranging from 600 to 700 cm^{-1}. Evidently, in the case of interest those features were only observed in the spectra of samples T5–T8, their intensity being lower than that of the peaks at $\sim$800 cm^{-1}. Thus, the tantalum in our films with $x \geqslant 2.3$ was predominantly five-fold coordinated. An exception is the film T8, in which the features at $\sim$600 and $\sim$800 cm^{-1} were weak, yet a peak at $\sim$480 cm^{-1} was observed. In [27], a close feature at wavenumber $\sim$500 cm^{-1} was observed (peak E in Takashi Tsuchiya study, figure 4(a)). However, this feature was always observed simultaneously with more intense peaks at $\sim$650 cm^{-1}, presumably due to the Ta–O valence vibrations in the case in which the tantalum atoms were six-coordinated ones. In the case of interest, for film T8 the peak at $\sim$480 cm^{-1} was a prevailing one. It can be assumed that this peak originated from the vibrations of Ta–O bonds, in the case in which the coordination number of tantalum atoms exceeded six. From the table, it is seen that the experimental values of the stoichiometry parameter x for the films in samples T7 and T8 was 2.79 and 2.77, and it is in those films where the feature at $\sim$480 cm^{-1} was observed. The assumption that no tantalum atoms with coordination numbers in excess of six were present in such films calls for further study.

Let us turn now to the feature at $\sim$200 cm^{-1}. In the literature, no explicit hypotheses about the nature of this peak are available. In [27], it was suggested that could be a
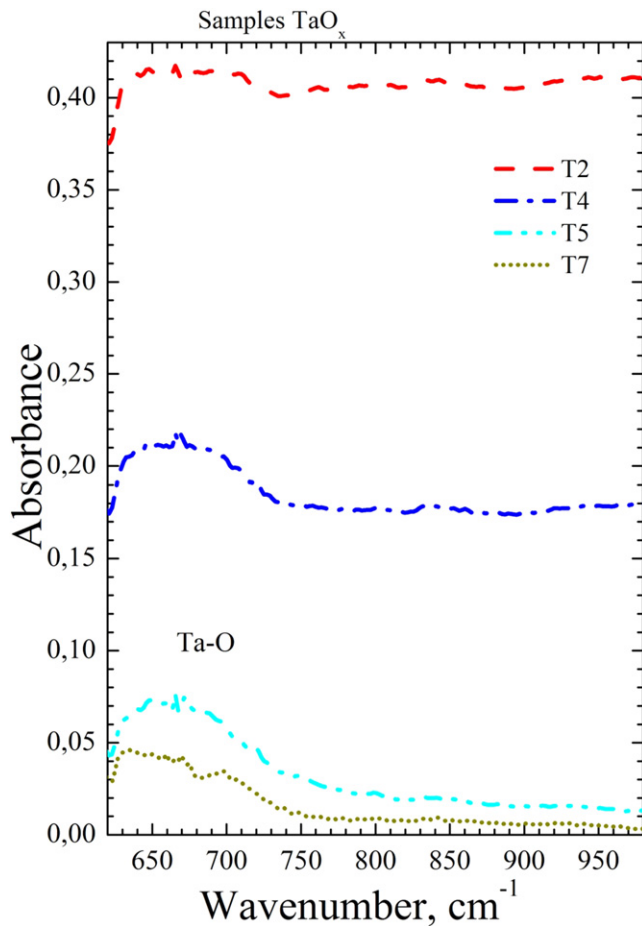
Figure 8. IR absorbance spectra of TaO$_x$ films (Si substrate was a reference sample).

contribution due to the vibrations of Ta–Ta bonds. However, those peaks were almost absent from the spectra of the films with the highest tantalum contents (T1–T3). We believe that that peak could be a contribution due to phonons localized in tantalum nanoclusters or, alternatively, it could be a contribution due to the interfacial phonons at the boundaries of tantalum clusters. It is seen that, on decreasing the partial pressure due to oxygen, this acoustic peak increased in amplitude and exhibited a shift. The only exception from the observed regularity was the sample T8. This matter calls for further study. For the time being, the emergence of the acoustic 'shoulder' at ~200 cm^{-1} can be tentatively attributed to the tantalum clusters present in the films.

Figure 8 shows the IR absorption spectra of TaO$_x$ films. The virgin Si substrate was used as a reference when measuring FTIR absorbance spectra. The spectra are dominated by a main line at about 670 cm^{-1} which (according to Raman spectra) could be associated with the Ta–O vibrations, band D in [27]. It should be noted that in samples T2 and T4 (metal-rich materials) there is absorption background in all studied range. It can be due to absorption in metallic clusters. In samples T5 and T7 (more oxygen) the Ta–O vibration peak is more pronounced. The large width of the peak indicates that in the films there are regions with different local stoichiometric compositions.

Thus, the data obtained indicate nanoscale fluctuations in the stoichiometric composition of the TaO$_x$ films, which stimulates attempts to construct a structural model of films different from well-known RB and RM. Rather, it is some intermediate model.

The intermediate model of structure and nanoscale potential fluctuation in TaO$_x$

The Ta$_2$O$_5$ consists of TaO(6) structural units. The replacement of one O atom with a Ta atom results in the formation of a TaTaO(5) structural unit, whereas the replacement of two, three, or four O atoms with two, three, or four Ta atoms yields TaTa(2)O(4), TaTa(3)O(3), or TaTa(4)O(2) structural units, respectively. Hypothetically, in a similar manner, TaTa(5)O, and TaTa(6) structural units can be formed. However, the replacement of more than four O atoms with Ta atoms turns out to be impossible because of Ta atomic radii 2.09 Å too high (for comparison radii of the O atom is 0.48 Å). In the RB model, TaO$_x$ consist of a mixture of TaTa(υ)O(6-υ) structural units with $\upsilon = 0, 1, 2, 3, 4,$ 5 and 6. Such a model fails to describe the TaO$_x$ structure. In the RM model, TaO$_x$ presents a mixture of Ta$_2$O$_5$ and Ta. The experiment points to the presence of Ta$_2$O$_5$ and Ta in TaO$_x$; however, XPS and Raman scattering data point to the occurrence of TaO$_y$ suboxides involving TaTa(υ)O(6-υ) structural units as well. Thus, neither the RB nor the RM models adequately describes the structure of TaO$_x$. The TaO$_x$ consists of TaTa(υ)O (6-υ), $\upsilon = 0, 1, 2, 3, 4, 5$ and 6 structural units; however, the distribution of the structural units in the material is not a random one like the distribution that appears in the RB model. We call proposed model structure as intermediate model.

According to the XPS, spectral ellipsometry and Raman data, TaO$_x$ consists of Ta$_2$O$_5$, Ta and TaO$_y$ suboxides. TaO$_y$ may appear at the Ta$_2$O$_5$/Ta interface, in the volume of Ta$_2$O$_5$ and in the volume of the Ta. A two-dimensional representation of the TaO$_x$ atomic structure in the intermediate model as well as the band diagram of TaO$_x$ are shown in figure 9. The electron affinity of Ta$_2$O$_5$ is $\chi = 3.3$ eV. The work function of metallic Ta is 4.4 eV. Spatial fluctuations of the chemical composition give rise to the local spatial fluctuations of the bandgap energy in TaO$_x$. Thus, E_g in TaO$_x$ varies in the range from 0 to 4.2 eV. The conduction-band edge position E_c, with respect to the electron energy in vacuum E_0, varies in the range from 3.3 to 4.4 eV. These quantities define the maximum fluctuation scale (1.1 eV) of E_c in TaO$_x$. The energy position of E_v with respect to the E_0, varies in the range from 4.4 to 7.5 eV. The height of the potential barrier for holes at the Ta/Ta$_2$O$_5$ interface defines the maximum fluctuation scale (3.1 eV) of the valence-band top position E_v in TaO$_x$. According to the FESEM structural measurements, the typical spatial scale of potential fluctuations in TaO$_x$ falls into the range less than 20 nm (see figure 1).

The proposed model of potential fluctuations is based on the nonstoichiometry of TaO$_x$. Local spatial fluctuations of the potential lead to local spatial variations in the bandgap in the range 0–4.2 eV. As a result, potential wells are formed for electrons and holes. Similar local spatial fluctuations of potential are observed in heavily doped semiconductors. In this case, the potential fluctuations are due to spatial fluctuations of
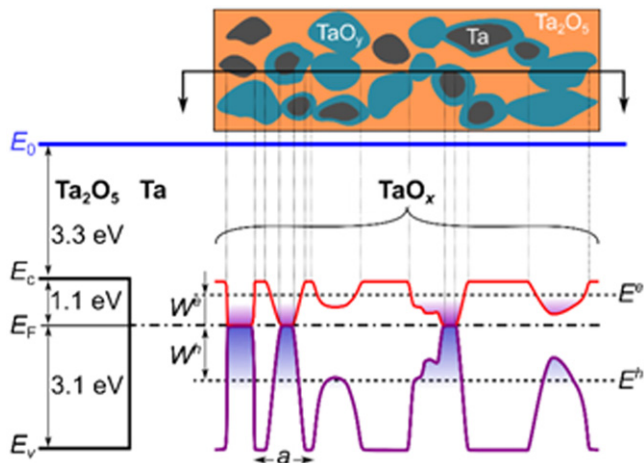
Figure 9. The intermediate model of nanoscale potential fluctuations in nonstoichiometric TaO$_x$. Two-dimensional model for the atomic structure of TaO$_x$ (on top) and it energy diagram with the Ta/Ta$_2$O$_5$ interface (below): the blue solid line shows the electron energy with respect to one in vacuum E_0, and the dash-and-dot line shows the position of Fermi level E_F in Ta. ≪a≫ is the characteristic spatial scale of potential fluctuations. E^e and E^h are the percolation levels for electrons and holes; W^e and W^h are the barriers for excitation of electrons and holes from the Fermi level to the electron and hole percolation levels, respectively.

concentration of charged donors and acceptors, so, the potential fluctuations have an electrostatic nature, while the width of the bandgap remains unchanged. The TaO$_x$ is quasineutral, the average electric charge is zero in every local volume. So, unlike to heavily doped semiconductors, in TaO$_x$ at each point of space the electric field for an electron and a hole has the opposite direction (figure 9). In the proposed model of nanoscale potential fluctuations, the conductivity of TaO$_x$ is due to the contribution of both electrons and holes. The electronic conductivity of TaO$_x$ is due to electrons that are excited from the Fermi level to the electronic percolation level. The hole conductivity of TaO$_x$ is due to holes that are excited from the Fermi level to the hole percolation level (figure 9).

The possibility of using TaO$_x$ as a storage medium in CTF memory

The operating principle of state-of-the-art flash memory devices is based on the accumulation (localization) of electrons or holes at deep traps in silicon nitride [31, 32]. The lifetime of electrons and holes in localized states should be up to 10 years at temperature 85 °C. According to figure 9, metallic tantalum nanoclusters in a Ta$_2$O$_5$ matrix act as deep potential wells (traps) for contact-injected electrons and holes. Thus, there arises a possibility to use nonstoichiometric metal-enriched TaO$_x$, as the storage medium in flash memory elements, instead of silicon nitride (figure 10). The depth of the potential wells due to metallic Ta for electrons and holes in TaO$_x$ is 1.1 eV and 3.1 eV, respectively (figure 9). Thus, it can be expected that the potential wells due to metallic Ta in TaO$_x$ will can ensure a giant retention time, or giant lifetime of electrons/holes in localized states.
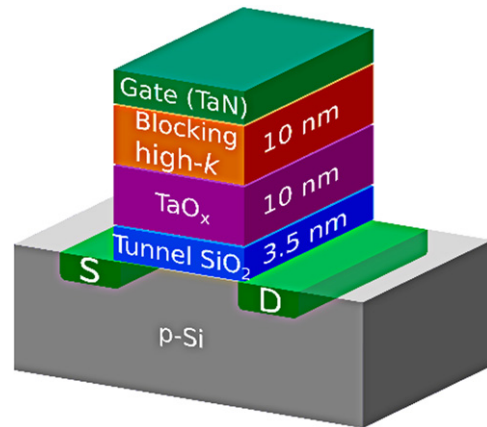

Figure 10. A flash memory element using TaO$_x$ as the storage medium.

The advantage of TaO$_x$-based flash memory compared with silicon nitride-based memory is based on the fact that TaO$_x$ has a higher dielectric constant (20) than the dielectric constant of silicon nitride (7). It was shown by Zhu *et al* [33] that memory based on tantalum oxide, due to higher dielectric constant, has a higher range of information retention time.

The flash memory element is similar to the traditional field-effect transistor in which, instead of the gate dielectric, a three-layer dielectric is used (figure 10). The Si substrate is *p*-type, the source (S) and drain (D) areas are *n*-type (figure 10). A thermally grown 3.5 nm thick SiO$_2$ layer functions as the tunnel dielectric. Over the tunnel oxide, a 10 nm thick storage layer of TaO$_x$ is provided. Over the storage dielectric, a low-conducting blocking high-κ dielectric is used. As the latter dielectric, Al$_2$O$_3$ is appropriate for use [31]. Tantalum nitride TaN is normally used in state-of-the-art flash memory elements as a conducting gate.

Conclusions

In the present study, the structure of nonstoichiometric metal-enriched tantalum oxide films of different compositions were investigated by means of electron microscopy, XPS and optic methods. It was found that TaO$_x$ films consist of Ta$_2$O$_5$, metallic Ta clusters, and tantalum suboxides enriched with tantalum TaO$_{y<2.5}$. The presence of Ta$_2$O$_5$ in our samples was confirmed by the observation of the Raman peak at about 800 cm^{-1}. The presence of metallic Ta clusters was also confirmed by the analysis of Raman spectra as the involvement of peaks at 200 cm^{-1}. According to electron microscopy data, the sizes of the metallic Ta nanoclusters in our samples were less than 20 nm.

Thus, the structure of TaO$_x$ cannot be described within the framework of the RM model, nor can it be understood within the RB model. Based on our data, the intermediate model for the TaO$_x$ atomic structure was proposed and justified. Local spatial fluctuations of the chemical composition of TaO$_x$ lead to spatial fluctuations in the bandgap. The localization of electrons and holes in TaO$_x$ occurs in Ta metallic nanoclusters. A new flash memory element is proposed, in which the TaO$_x$ layer acts as a storage medium.

Acknowledgments

ORCID iDs

Vladimir A Gritsenko ® https://orcid.org/0000-0003-1646-0848
Vladimir A Volodin ® https://orcid.org/0000-0002-1431-8242
Timofey V Perevalov ® https://orcid.org/0000-0003-0895-6202
Vladimir N Kruchinin ® https://orcid.org/0000-0002-9905-9031
Alina K Gerasimova ® https://orcid.org/0000-0003-2932-8424
Vladimir Sh Aliev ® https://orcid.org/0000-0002-4266-971X
Igor P Prosvirin ® https://orcid.org/0000-0002-0351-5128

References

[1] Wilk G D, Wallace R M and Anthony J M 2001 High-κ gate dielectrics: current status and materials properties considerations *J. Appl. Phys.* **89** 5243–75

[2] Robertson J 2004 High dielectric constant oxides *Eur. Phys. J. Appl. Phys.* **28** 265–91

[3] Perevalov T V and Gritsenko V A 2010 Application and electronic structure of high-κ dielectrics *Phys. Usp.* **180** 561–75

[4] Robertson J and Wallace R M 2015 High-κ materials and metal gates for CMOS applications *Mater. Sci. Eng.* R **88** 1–41

[5] Zhu H, Bonevich J E, Li H, Richter C A, Yuan H, Kirillov O and Li Q 2014 Discrete charge states in nanowire flash memory with multiple Ta_2O_5 charge-trapping stacks *Appl. Phys. Lett.* **104** 233504

[6] Lee M *et al* 2011 A fast, high-endurance and scalable non-volatile memory device made from asymmetric Ta_2O_{5-x}/TaO_{2-x} bilayer structures *Nat. Mater.* **10** 625–30

[7] Wang Z *et al* 2017 Memristors with diffusive dynamics as synaptic emulators for neuromorphic computing *Nat. Mater.* **16** 101–10

[8] Wedig A *et al* Nanoscale cation motion in TaO_x, HfO_x and TiO_x memristive systems *Nat. Nanotechnol.* 2016 **11** 67–75

[9] Egorov K V, Kuzmichev D S, Chizhov P S, Lebedinskii Y Y, Hwang C S and Markeev A M 2017 *In situ* control of oxygen vacancies in TaO_x thin films via plasma-enhanced atomic layer deposition for resistive switching memory applications *ACS Appl. Mater. Interfaces* **9** 13286–92

[10] Gritsenko V A, Perevalov T V, Voronkovskii V A, Gismatulin A A, Kruchinin V N, Aliev V S, Pustovarov V A, Prosvirin I P and Roizin Y 2018 Charge transport and the nature of traps in oxygen deficient tantalum oxide *ACS Appl. Mater. Interfaces* **10** 3769–75

[11] Islamov D R, Gritsenko V A, Cheng C H and Chin A 2014 Percolation conductivity in hafnium sub-oxides *Appl. Phys. Lett.* **105** 262903

[12] Orlov O M, Krasnikov G Y, Gritsenko V A, Kruchinin V N, Perevalov T V, Aliev V S, Islamov D R and Prosvirin I P 2015 Nanoscale potential fluctuation in non-stoichiometric hafnium suboxides *ECS Trans.* **69** 237–41

[13] Gritsenko V A, Perevalov T V and Islamov D R 2016 Electronic properties of hafnium oxide: a contribution from defects and traps *Phys. Rep.* **613** 1–20

[14] Tsuchiya T, Imai H, Miyoshi S, Glans P A, Guo J H and Yamaguchi S 2011 X-ray absorption, photoemission spectroscopy, and Raman scattering analysis of amorphous tantalum oxide with a large extent of oxygen nonstoichiometry *Phys. Chem. Chem. Phys.* **13** 17013–8

[15] Gritsenko V A 2008 Atomic structure of amorphous non-stoichiometric silicon oxides and nitrides *Phys. Usp.* **178** 699–708

[16] Rykhlitskii S V, Spesivtrev E V, Shvets V A and Prokopiev V Y 2012 ELLIPS-1891-SAG spectral ellipsometric complex *Pribory Tekhn. Experimenta (in Russian)* **2** 161–2

[17] Adachi S 1999 *Optical Constants of Crystalline and Amorphous Semiconductors: Numerical Data and Graphical Information* (New York: Springer)

[18] Tompkins H and Irene E A 2005 *Handbook of Ellipsometry* (Berlin: Springer)

[19] Amirtharaj P M 1991 *Handbook of Optical Constants of Solids* ed D Palik (Amsterdam: Elsevier)

[20] Giannozzi P *et al* 2009 QUANTUM ESPRESSO: a modular and open-source software project for quantum simulations of materials *J. Phys.: Condens. Matter* **21** 395502

[21] Lee S H, Kim J, Kim S J, Kim S and Park G S 2013 Hidden structural order in orthorhombic Ta_2O_5 *Phys. Rev. Lett.* **110** 235502

[22] Guo Y Z and Robertson J 2015 Comparison of oxygen vacancy defects in crystalline and amorphous Ta_2O_5 *Microelectron. Eng.* **147** 254–9

[23] Atanassova E and Spassov D 1998 X-ray photoelectron spectroscopy of thermal thin Ta_2O_5 films on Si *Appl. Surf. Sci.* **135** 71–82

[24] Aliev V S, Gerasimova A K, Kruchinin V N, Gritsenko V A, Prosvirin I P and Badmaeva I A 2016 The atomic structure and chemical composition of HfO_x ($x < 2$) films prepared by ion-beam sputtering deposition *Mater. Res. Express* **3** 085008

[25] Shvets V A, Aliev V S, Gritsenko D V, Shaimeev S S, Fedosenko E V, Rykhlitski S V, Atuchin V V, Tapilin V M and Wong H 2008 Electronic structure and charge transport properties of amorphous Ta_2O_5 films *J. Non-Cryst. Solids* **354** 3025–32

[26] Perevalov T V and Shaposhnikov A V 2013 *Ab initio* simulation of the electronic structure of the crystalline modifications of Ta_2O_5 *J. Exp. Theor. Phys.* **116** 995–1001

[27] Tsuchiya T, Imai H, Miyoshi S, Glans P A, Guo J and Yamaguchi S 2011 X-ray absorption, photoemission spectroscopy, and Raman scattering analysis of amorphous tantalum oxide with a large extent of oxygen non-stoichiometry *Phys. Chem. Chem. Phys.* **13** 17013–8

[28] Joseph C, Bourson P and Fontana M D 2012 Amorphous to crystalline transformation in Ta_2O_5 studied by Raman spectroscopy *J. Raman Spectrosc.* **43** 1146–50

[29] Balachandran U and Eror N G 1982 A study of the crystal structure of B-Ta_2O_5 by vibrational spectroscopy and x-ray diffraction *J. Mater. Sci. Lett.* **1** 219–22

[30] Dobal P S, Katiyar R S, Jiang Y, Guo R and Bhalla A S 2000 Raman scattering study of a phase transition in tantalum pentoxide *J. Raman Spectrosc.* **31** 1061–5

[31] Gritsenko V A 2016 *Thin Films on Si: Electronic and Photonic Applications* ed V Narayanan *et al* (Singapore: World Scientific Press)

[32] Prince B 2014 *Vertical 3D Memory Technologies* (New York: Wiley)

[33] Zhu H, Bonevich J E, Li H, Richter C A, Yuan H, Kirillov O and Li Q 2014 Discrete charge states in nanowire flash memory with multiple Ta_2O_5 charge-trapping stacks *Appl. Phys. Lett.* **104** 233504